Mustang detectors – Array2

Simon Dicker, Phil Korngut, Brian Mason & James Aguirre

Feb 7, 2007

1. Introduction.

Mustang suffers from excess noise at high and low frequencies. Since August 2006 we have had a fully functioning array read out using the Mark III electronics. In the fall Mustang achieved first light on the GBT. During this engineering run, simultaneous functionality of all system components was demonstrated, proving the run a success. However, extraneous in band noise introduced in the detector loop limited observations to only the brightest 3mm sources in the sky. The objects observed emit between 100 and 1000 times more flux than most targets of scientific interest. It is clear that in order to produce the cutting edge science MUSTANG is capable of, the noise must be reduced towards the theoretical limit.

1.1. Noise characteristics

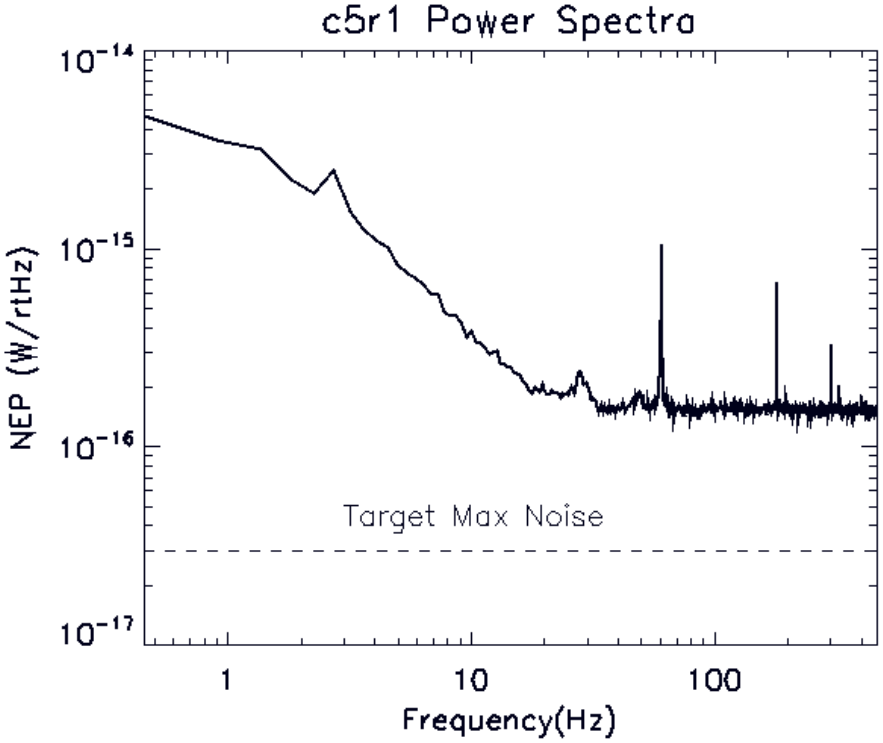

Figure 1: One of the better power spectra from a MUSTANG detector. Also shown on the graph is our target noise level. Features in the spectra include a high white noise floor, an excessive 1/f component, a 1.4Hz (2.8Hz is more visible) signal associated with the pulse tube and 60Hz (and its harmonics). Of particular concern is noise below 100Hz where most astronomy is located.

Figure 1 depicts the power spectrum of one of the better MUSTANG pixels. In the

1-2Hz band, the TES noise is roughly a factor of 100 greater than the maximum level predicted in proposals. Other pixels display spectra nearly a factor of 10 above this. While the 1/f component is responsible for the majority of this noise, the white noise level at frequencies above 50Hz is still roughly a factor of 8 above the desired limit.

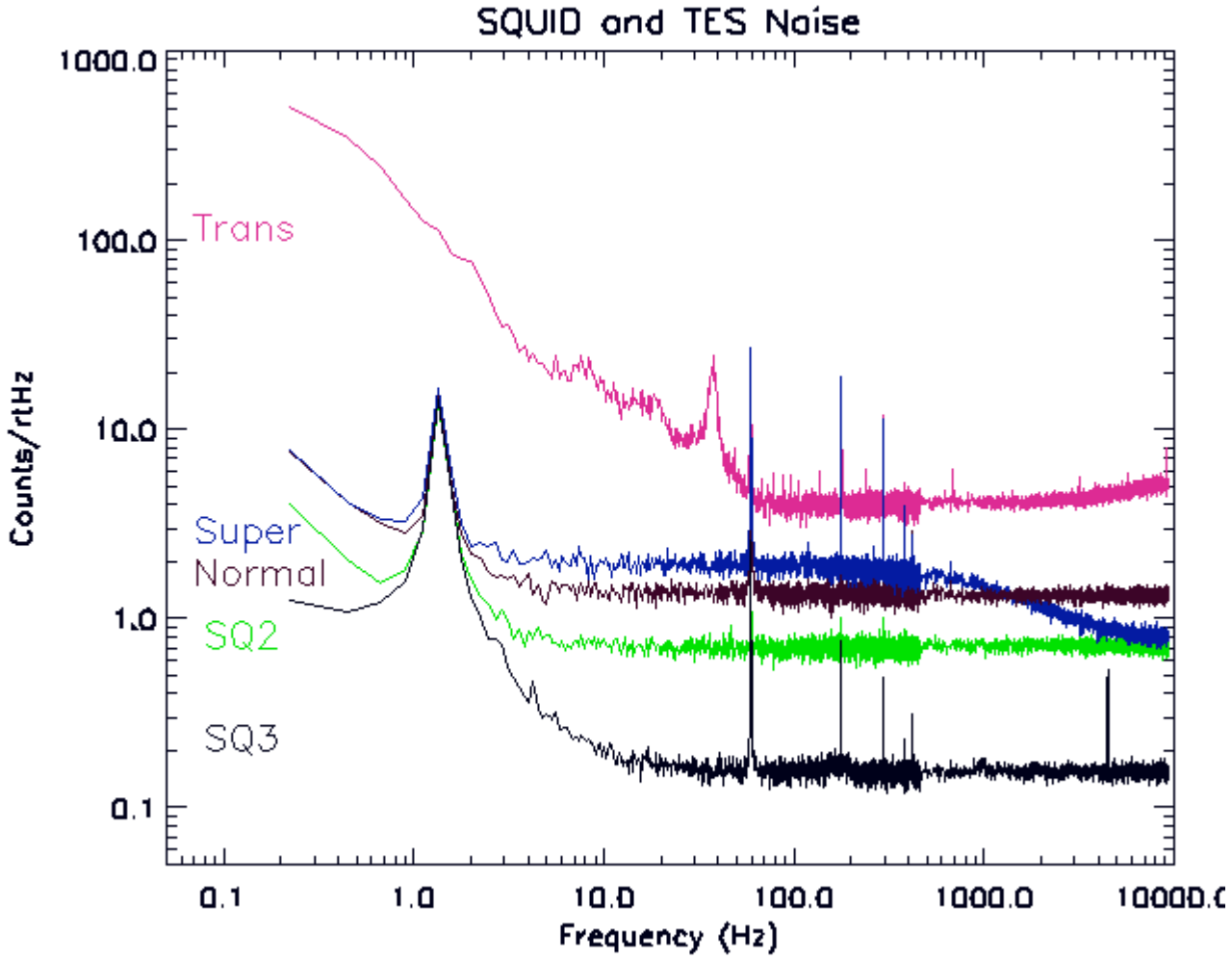

Figure 2: Noise power spectra of the SQUID readout electronics and a typical detector in its three thermal states.

Figure 2 displays the noise components introduced by each level of the readout electronics. It is clear that excess low frequency noise is only present in the detector loop when the TES is biased on its transition. Maximum MarkIII sampling rates were used to obtain these spectra. Unfortunately it is not fast enough to observe the L/R rolloffs of the detector loop in the normal and transition states. One does not expect to observe them in this frequency range as the normal state rolloff should be factor of 18 higher in frequency than that of the superconducting state (which rolls of at ~1kHz). The speed of the circuit is set by the bias resistor, TES and the input inductor to the first stage SQUID. Additional nyquist inductors had to be removed as they were observed to set up electrothermal oscillations.

2. **Making noise measurements.**

Noise measurements were made using the full Mark III electronics system with IRC software. A comparison of these spectra to those taken with a conventional analog spectrum analyzer proves the absence of artifacts introduced by the multiplexing or digital sampling systems. Such a comparison is displayed in figure 3.

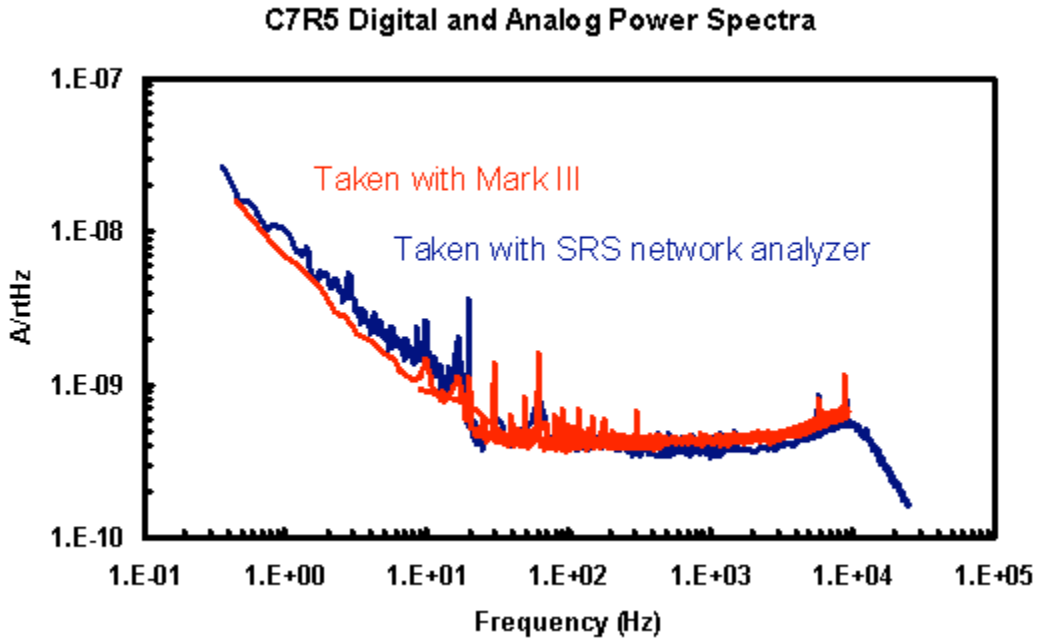

Figure 3: Comparison of power spectra taken with different methods. Red displays data taken through the Mark III system and blue data were obtained through an analog SRS network analyzer.

3. **Variations in noise.**

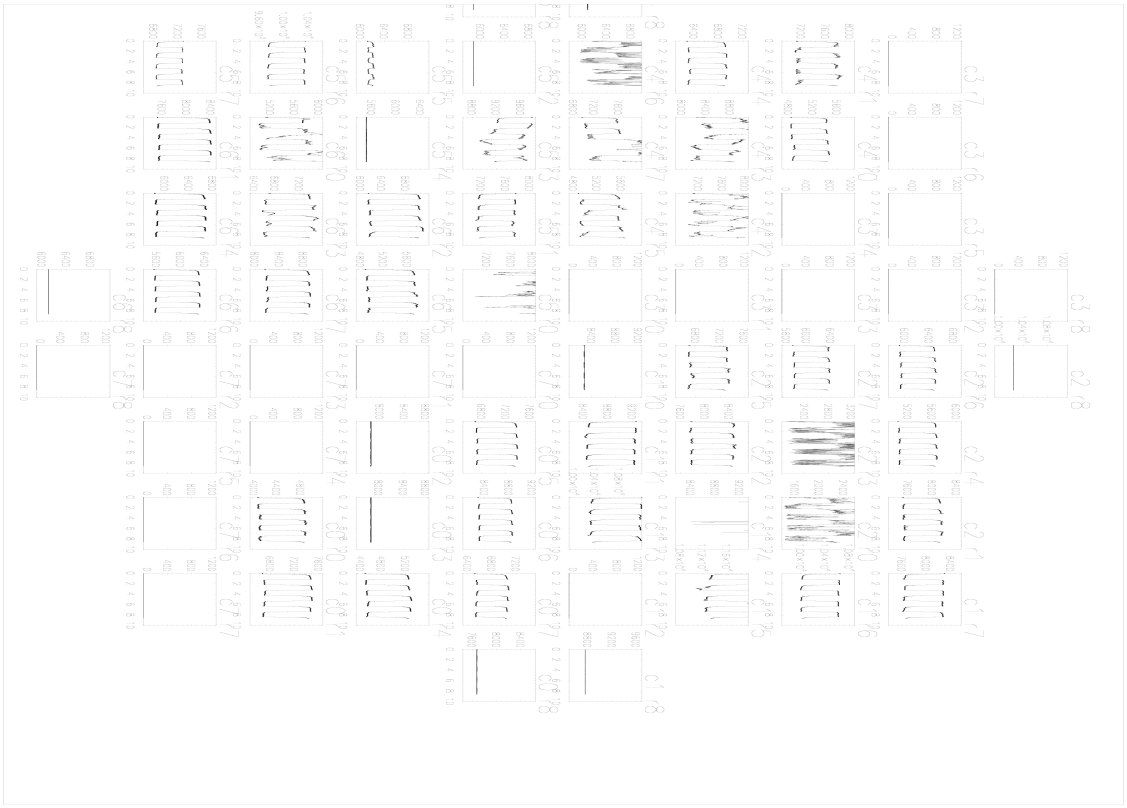

Figure 3

3.1. **Low frequency noise**

Scanning speed of the GBT and optical time constants of the detectors constrain MUSTANG astronomy to the 1-2 Hz band. For this reason, 1/f noise which cuts in at ~100 Hz limits our sensitivity to several orders of magnitude below the desired level.

Initially, this slow noise was thought to be attributable to system fluctuations. Possible candidates were: noise in the detector bias line, instabilities in the array baseplate temperature, variations in optical load or RFI. For reasons described in this section, all are deemed unlikely.

3.1.a ***Detector Bias Line***

The fundamental architecture of the Mark III system has but one detector bias line per column. Therefore, if fluctuations of this voltage were the primary cause of our 1/f, one would expect strong correlation between pixels in the same column. Figure 4 displays both the time and frequency domain noise characteristics of three detectors in column 0. It is clear from these plots that there is a large variation in the severity of the noise within an electrical column. Also note that features in the time stream of one pixel do not appear simultaneously in a neighbor's output. Because the multiplexed sampling is taking place on timescales ten thousand times faster than the observed variations, all features which are not common to all pixels in a column must originate in individual detector loops or first stage SQUIDs and can not come from shared detector bias or

readout electronics.

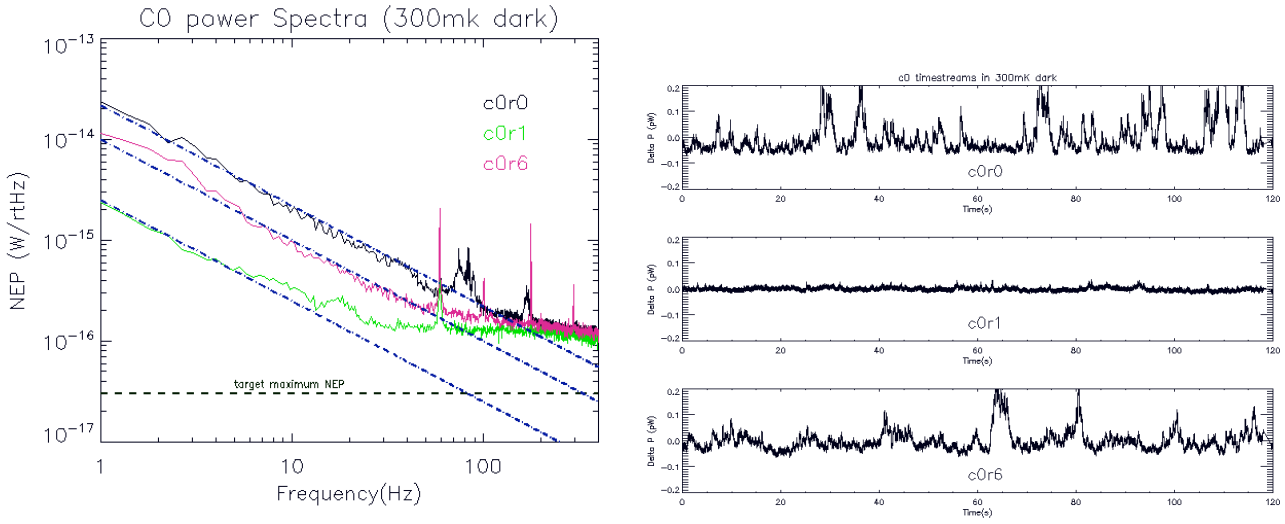

Figure 4: Time streams and power spectra for three pixels in column 0.

3.1.b ***Array Bath Temperature Variation***

A lack of pixel to pixel correlation is also strong evidence that baseplate temperature fluctuations are not the cause of excess low frequency noise. It is unphysical for the array to fluctuate at the individual detector level. The entire array is heatsunk to the He3 fridge through a single copper strap which all instabilities would have to propagate across. The only other feasible path one could introduce bath temperature fluctuations through is across the kevlar suspension system which the entire 300mK stage rests upon. Rough calculations suggest a thermal signal propagating across this system would be attenuated by hundreds of dBs by the time it reached the array package. Even if they were to be introduced via this method, some common mode noise is to be expected.

3.1.c ***Optical load variations***

Internally generated optical load fluctuations can not be considered. The noise is present with equivalent magnitudes when the array is blanked off at 300mK and when it is exposed to the entire optics cavity.

3.1.d ***RFI***

Interference from external sources has been shown to be an unlikely cause of excess low frequency noise. Identical characteristics have been observed in several radio environments such as the Penn lab, the Green Bank lab and on the telescope. It is also true that no attenuation is seen when the receiver is completely enclosed in a faraday cage.

RFI introduced in the readout electronics up to the first stage SQUIDs can not be considered as pixels which share amplifiers and bias cards display different

characteristics. It is also true that the addition of ferromagnetic eccosorb to all leads coming in and out of the array package provided no improvement to the noise.

3.2 Characteristics of 1/f noise

Currently, no model which describes all observed phenomena exists. However, much work characterizing the noise has been done.

The effect in question is only present when a pixel is biased on its transition as is conveyed by figure 2. It is found in every readable detector at varying levels. These facts along with the reasoning described in section 3.1 have led us to suspect the nature of the noise to be intrinsic to the detectors.

This effect has been observed at different levels on some detectors. Details of these variations are found in section ___. Naturally, the parameter responsible for these variations is of great interest. Attempts at correlating the 1/f noise to several variables is described in the following subsections.

3.2.a *Noise vs. Bias*

As was stated earlier, the excess noise is present only on the transition and appears to be equally dominant throughout this thermal state. The dependence of power spectra on detector bias across the transition is displayed below in figure 5.

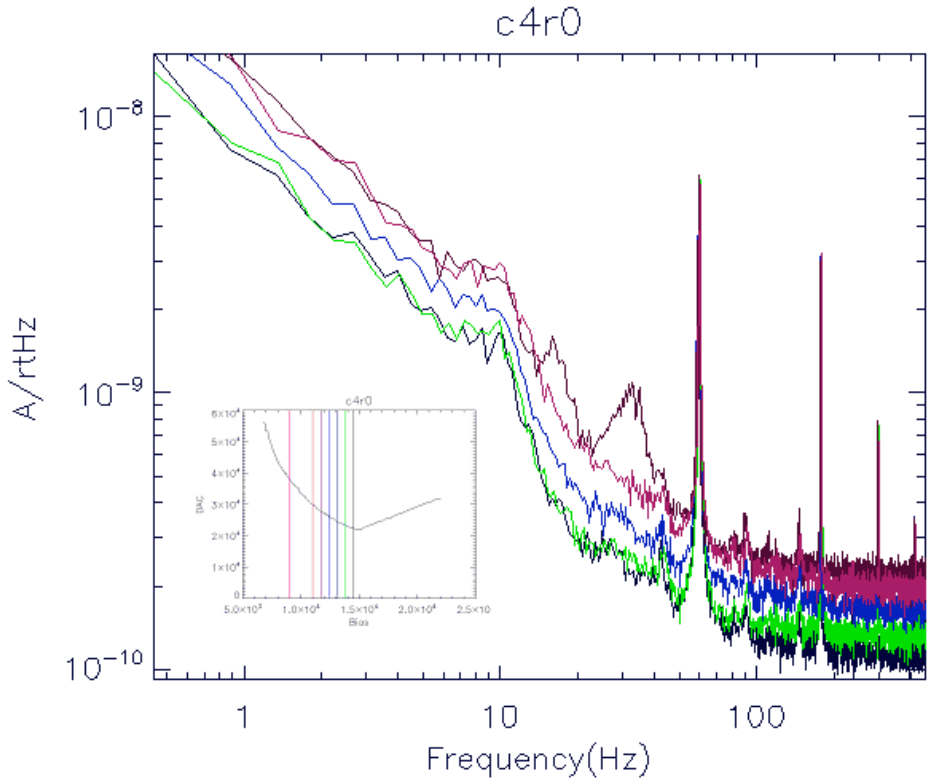

Figure 5: Dependence of noise on detector bias for c4r0. Inset displays relative location on an I(V) curve of each power spectrum.

As expected, detector current noise is observed to vary inversely with percent of normal TES resistance. However, the morphology of the power spectrum does not appear to vary. The white noise above 100Hz increases along with the 1/f and the frequency at which it begins does not change. There is no bias at which the effect is not present.

3.2.b ***Noise vs. Bath Temperature***

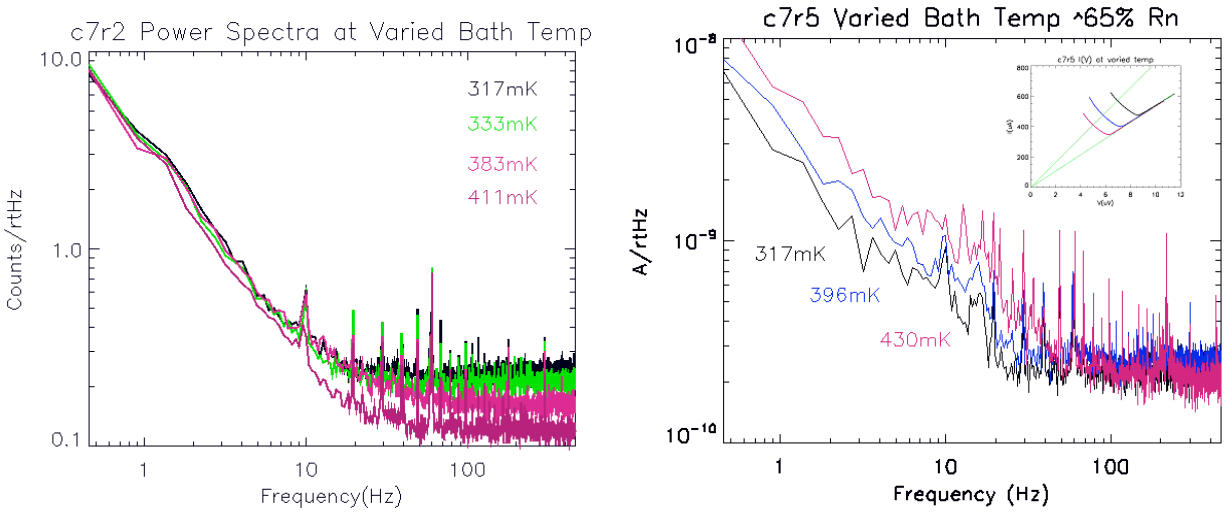

Figure 6a: power spectra of c7r2 at varied array baseplate temperatures and constant bias voltage. b:power spectra of c7r5 with varied array baseplate temperature at 65%Rn. Inset displays dependence of I(V) curves on bath temperature.

Bath temperature is the only variable shown to affect the 1/f noise differently than higher frequency white noise thus far. Figure 6a depicts the variability of a pixel's power spectrum when baseplate alone is varied. The white noise which dominates at frequencies higher than 40Hz is seen to decrease substantially as array temperature is increased while the 1/f remains constant. This can be attributed to an increase in TES resistance as an invariant bias voltage will place a detector higher on its transition when bath temperature is raised. When TES resistance is held constant with increased thermal power from the bath, the white noise holds at a constant level while the 1/f is increased. This effect is shown in figure 6b.

4. **Noise correlation.**

In the fall James Aguirre did a first characterization of the correlations in the MUSTANG data, and the effectiveness of a simple common-mode subtraction at removing them. The following two figures illustrate the principal conclusion, which is that while common mode subtraction helps—especially at the lowest frequencies-- there is a large, residual non-common mode excess power at medium to low frequencies (0.1 to 10 Hz, say).

-

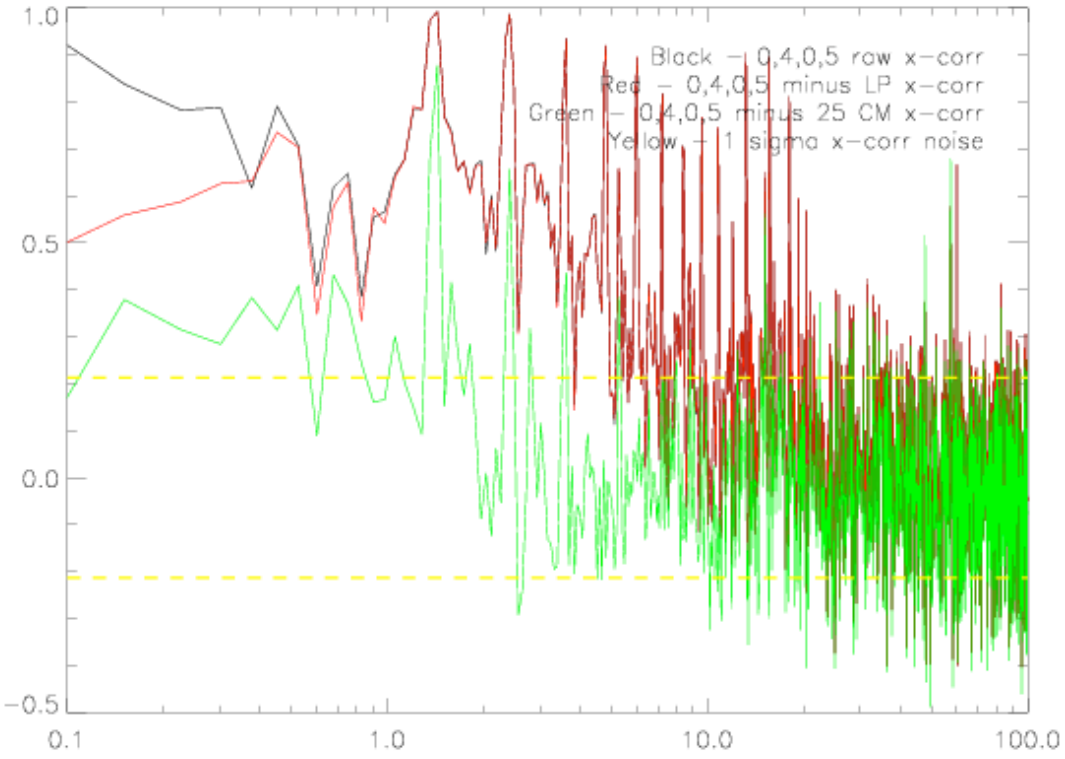

Cross power spectra for c0r4/c0r5 with a variety of data filtering strategies. Black is the raw cross power spectrum; red is the cross power spectrum after individual low-pas subtraction; green is the cross power spectrum after a 25-good-pixel common mode subtraction. Yellow lines are +/- 1 sigma stsatistical uncertainties on the estimates of individual cross-spectrum coefficients. These spectra are normalized by the autocorrelations to lie in the range +/-1. The fact that the green line is consistent with zero, roughly, above a couple of Hz indicates that the medium frequency correlations between c0r4 and c0r5 are well represented by the 25-pixel common mode. There is a significant correlation between c0r4 and c0r5 at frequencies less than 2 Hz which is not well-represented by the 25-pixel common mode.

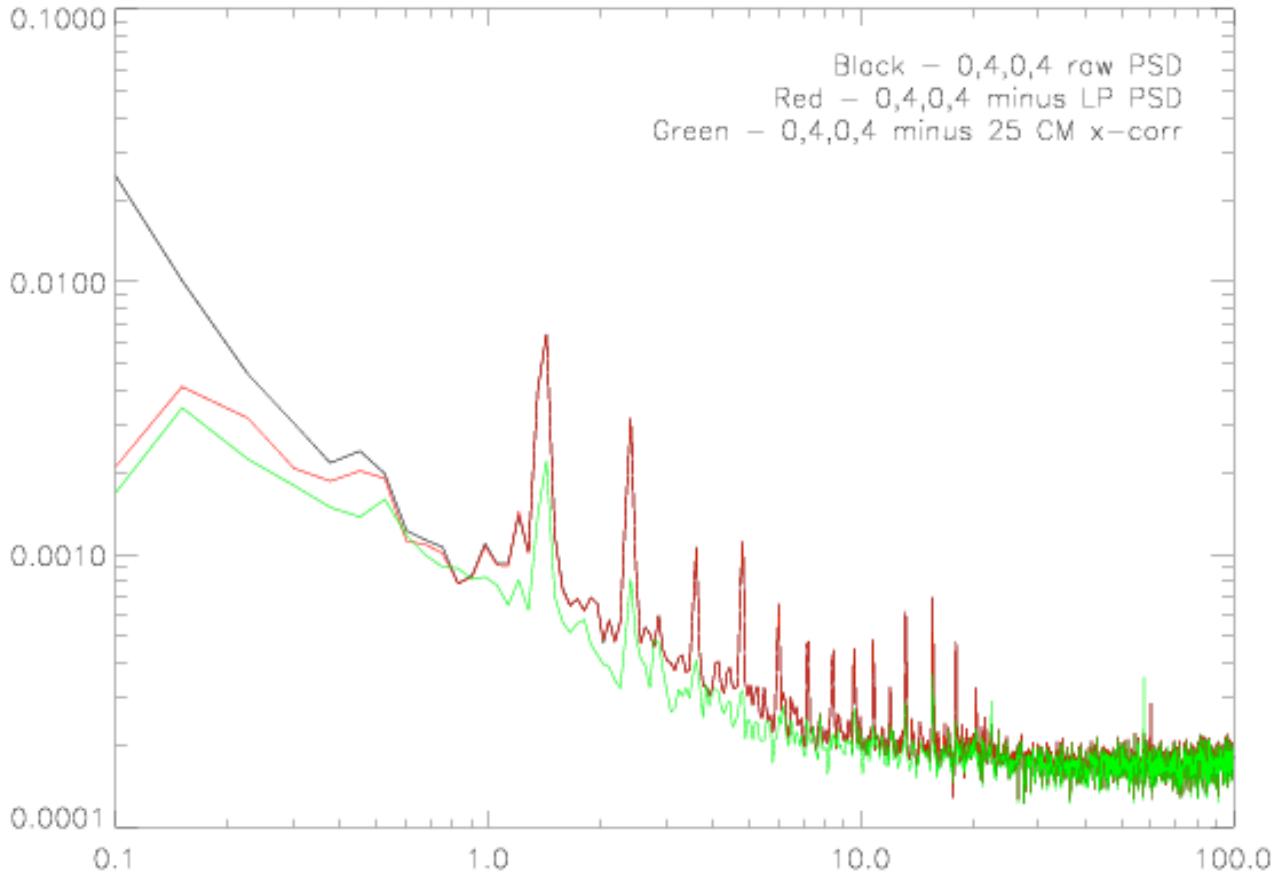

Noise power spectra for c0r5: raw (black); after low-pass filter subtraction (red); after 25-pixel common-mode subtraction (green). The fact that 1/f in the red and green traces remains, while the cross-correlations between c0r4 and c0r5 above 1 Hz are pretty small, is indicitave of uncorrelated 1/f noise.

We have also subjected a wide range of data from the lab and the telescope to Principal Component Analysis. The most important datasets are TPAR_02 scans 20, 21, and 49; TPAR_04 scans 54,55,73, & 74; TPAR_08 scan 70; and the series of 7 scans in the lab (300 mK dark) collected on 31jan07. The majority of the data analyzed were raw DAC timestreams, since the optical responsivity doesn't vary dramatically across the array and it appears unlikely that our systematics are photonic. For data where we had cal scans, standard filters were used to exclude grossly noisy pixels from the analysis.

Conclusions and hints resulting from this exercise are as follows:

- ***All of the principal components, except those dominated by dark squids, have strong 1/f power spectra under all conditions observed***. There is no indication that the 1/f is confined to one or a few linear combinations of pixels, as would be expected for loading fluctuations or baseplate temperature variations.
- A common mode is usually present as the first principal component. Aside from this, what you see are modes that mostly correspond to individual noisy detectors. Note that this is *after* rejecting the noisiest pixels. The pixels that stand out as noisy in one dataset do not necessarily stand out in another dataset, though over hours there is good coherence.
- We do **not** see prominent "individual column" or "individual row" principal components, as would be expected for certain electronics-related systematics.
- The eigenvectors obtained are generally repeatable scan-to-scan, indicating that the assumption that the basic instrument model (C_ij) is stable over the period analyzed is valid, and that non-gaussianity of the noise fluctuations isn't having a dramatic impact on our results.

As an example consider TPAR_02 s.49, a daisy scan on (essentially) blank sky. This is the first principal eigenvector, a common mode:

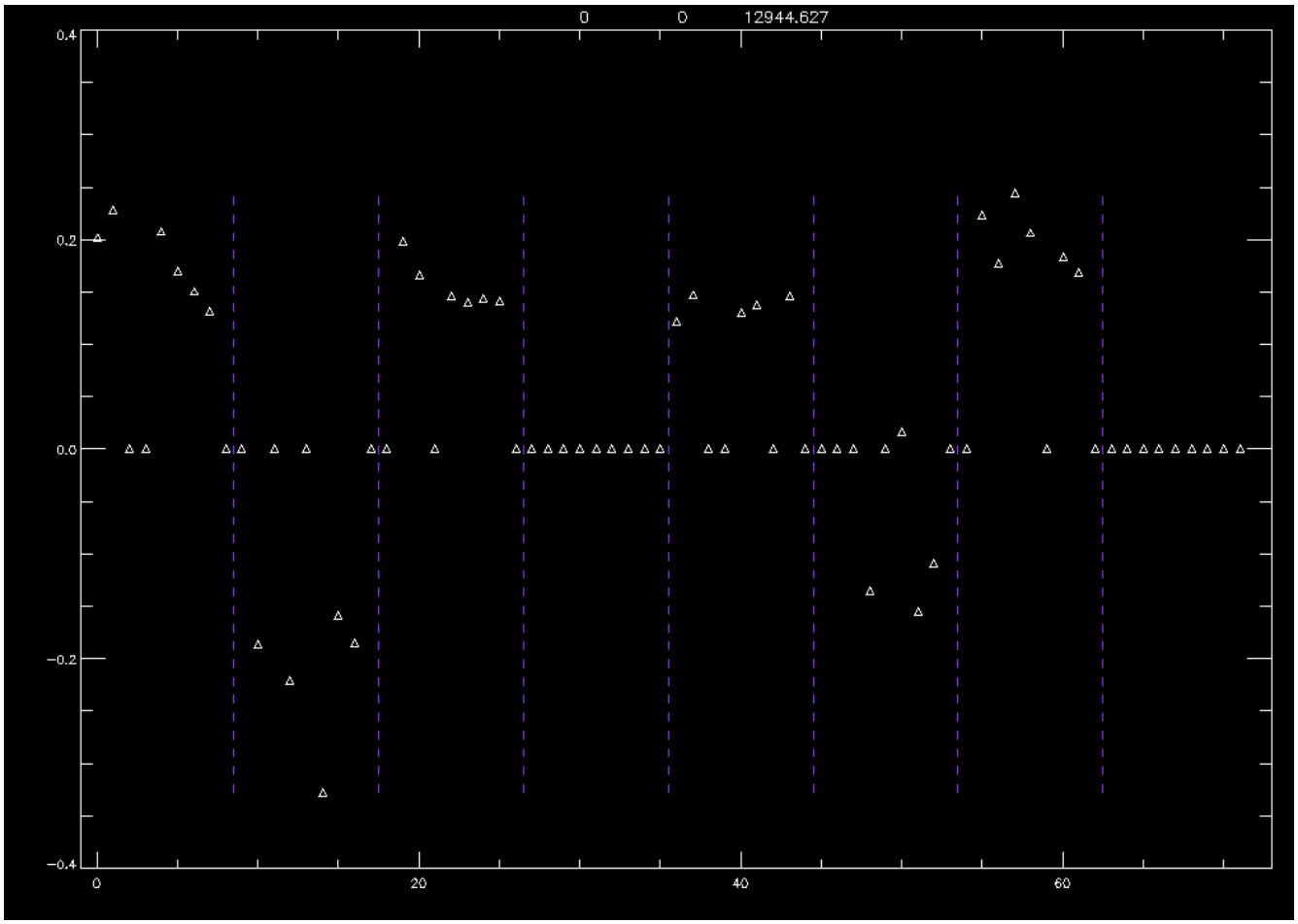

A few notes and observations:

- For those unfamiliar with PCA, the values of the individual coefficients reflect the coefficients multiplying individual detectors' data. In this case, these can be interpreted directly as the quantity of the common mode signal seen by the given pixel.
- Columns are separated by purpled dashed lines. within a column, rows go from 0-8.
- The signs are as expected for a common mode in uncalibrated data
- To check the mappings recall that: c0r2 and c0r3 are always dead; c5r5 is known to have a weak response opposite to the rest of c5. Column 3 is dead, column 7 is dead.

This is the second principal component, a typical "one noisy pixel" eigenvector:

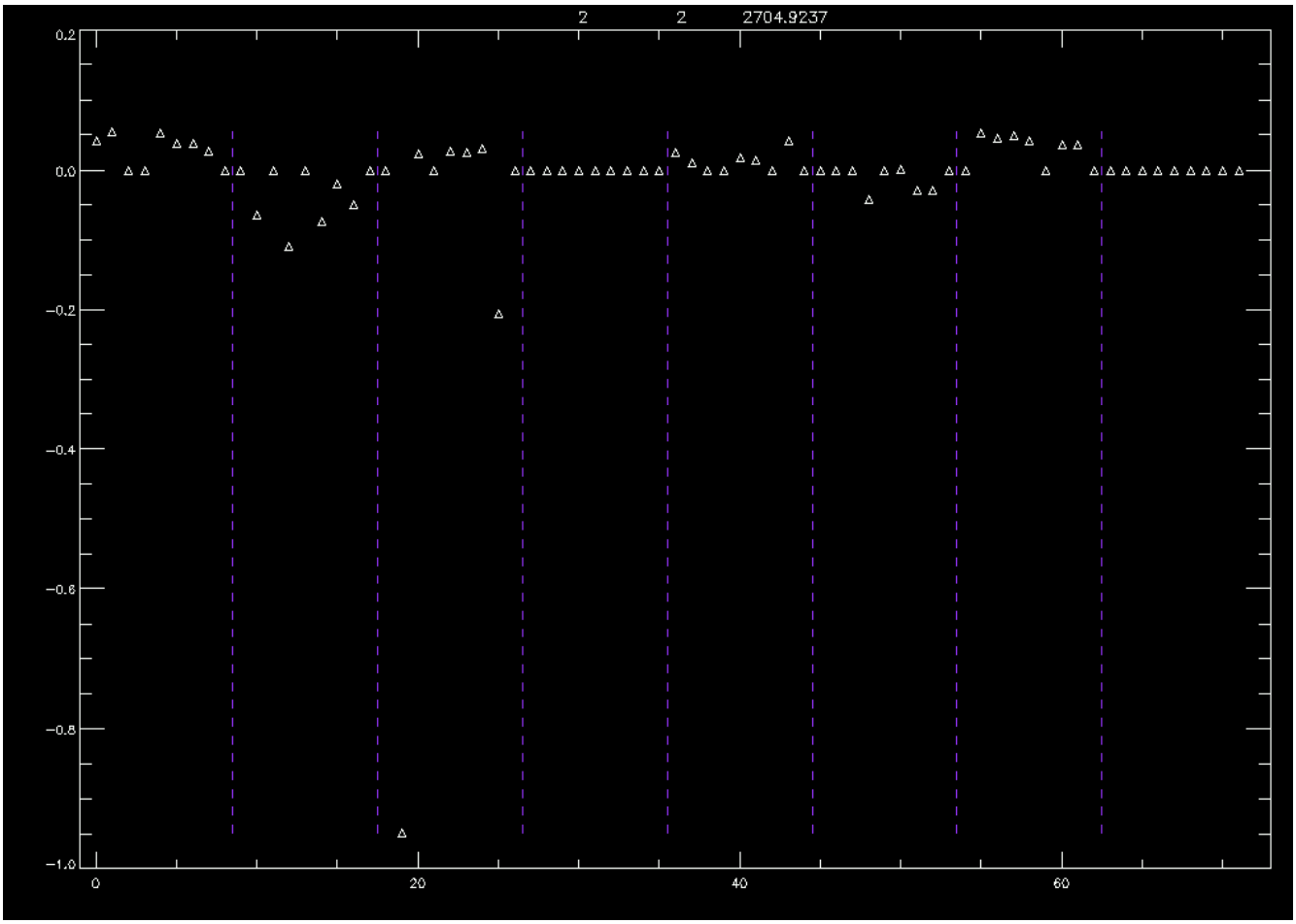

This is the third principal component:

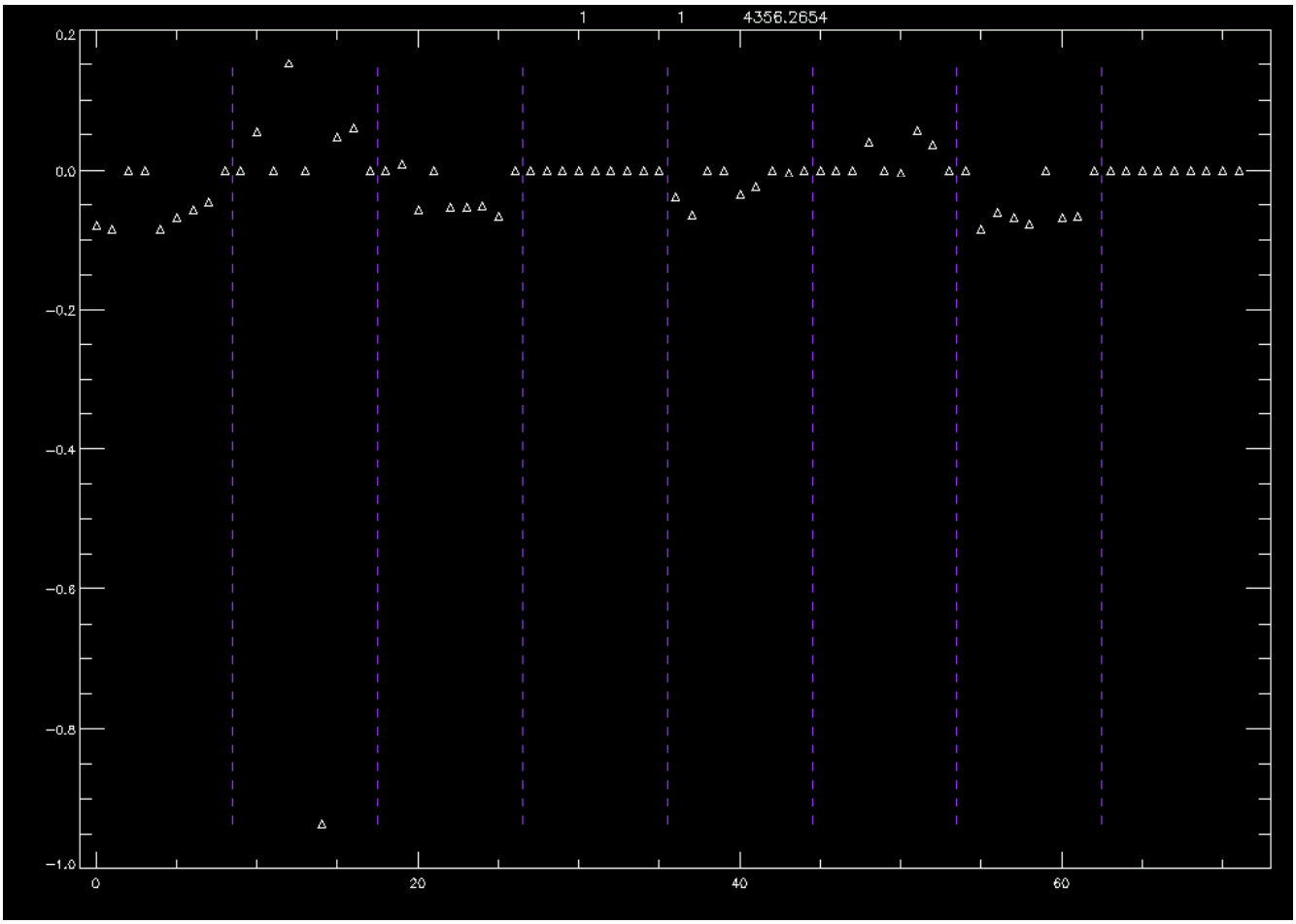

The power spectra of these linear combinations of data, in order, are:

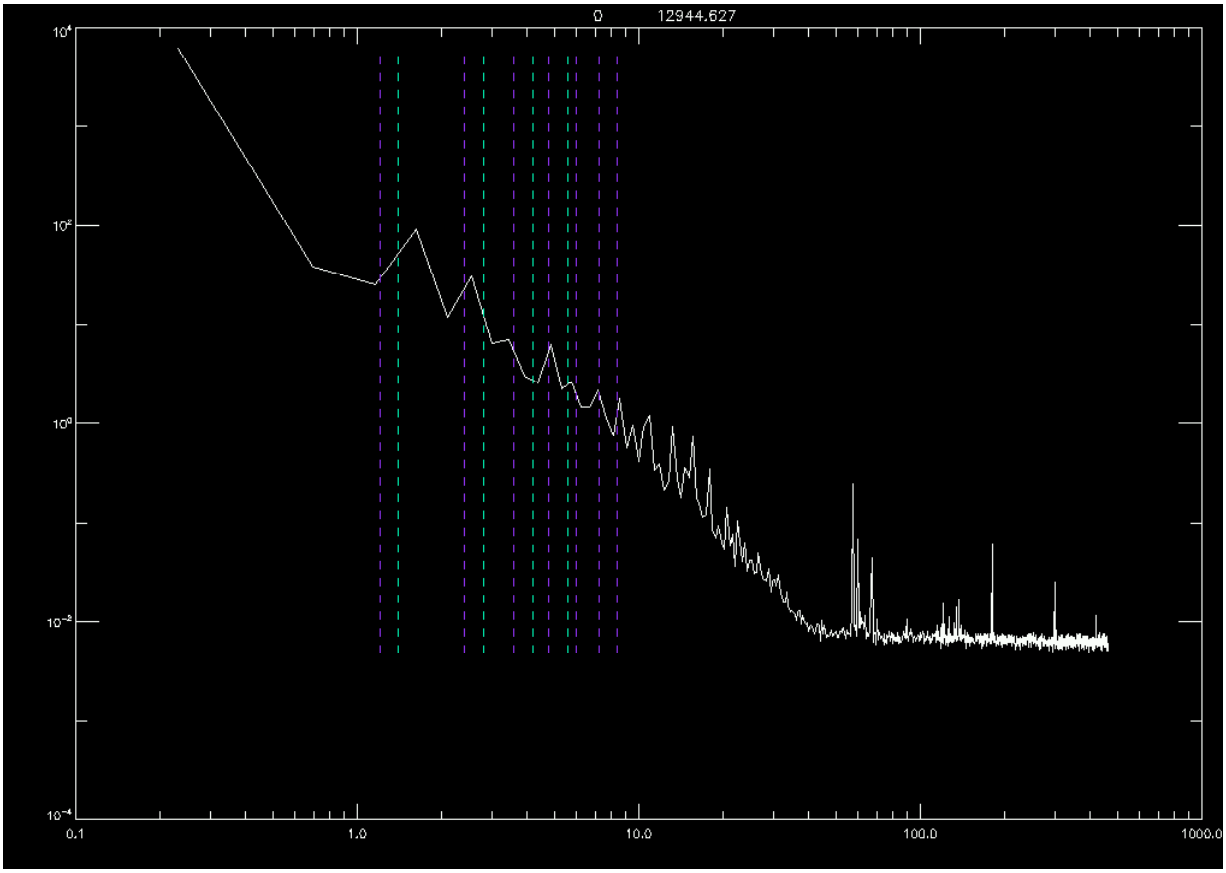

Power spectrum of TPAR_02 s.49, 1st PC

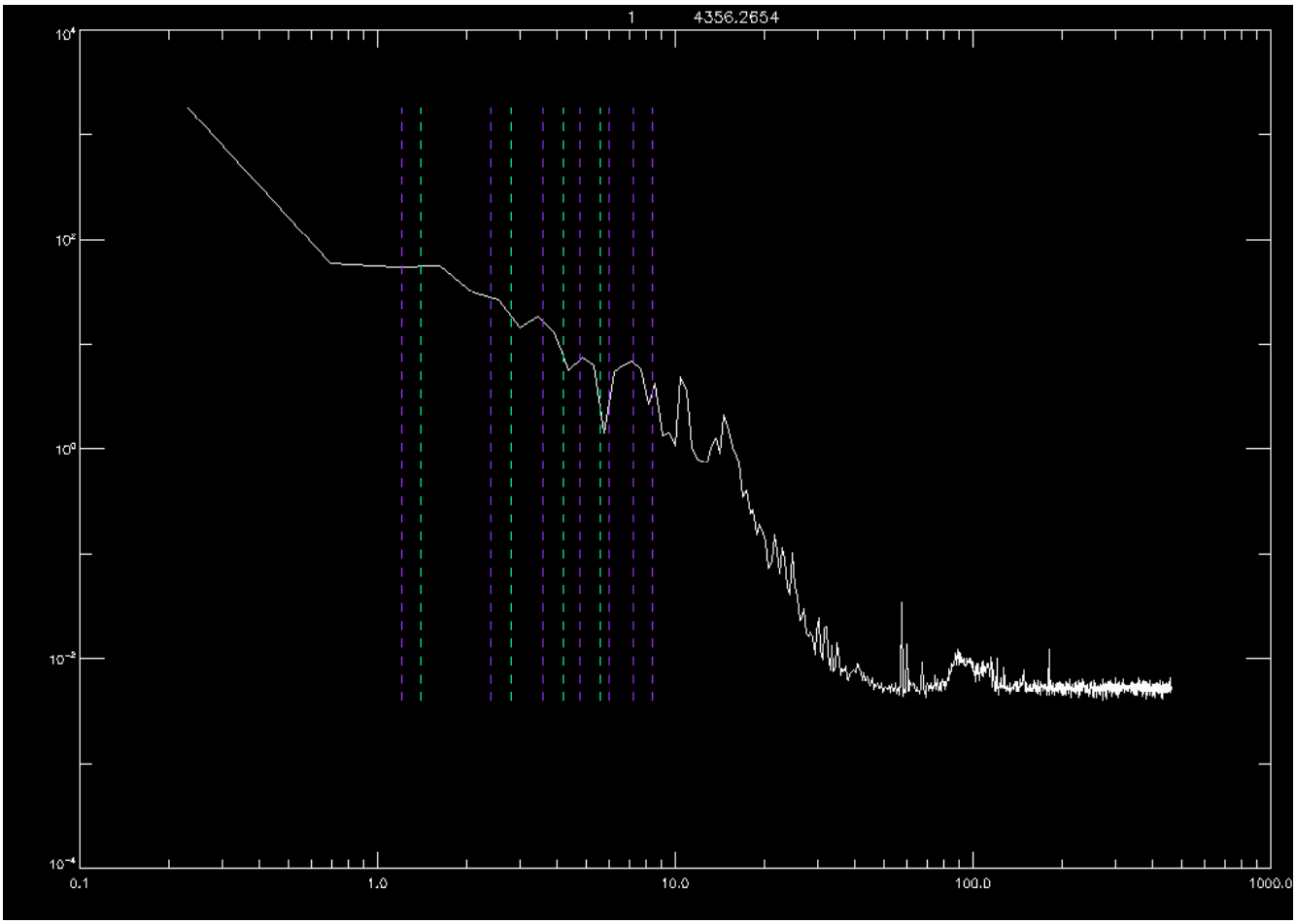

Power spectrum of TPAR_02 s.49, 2nd PC

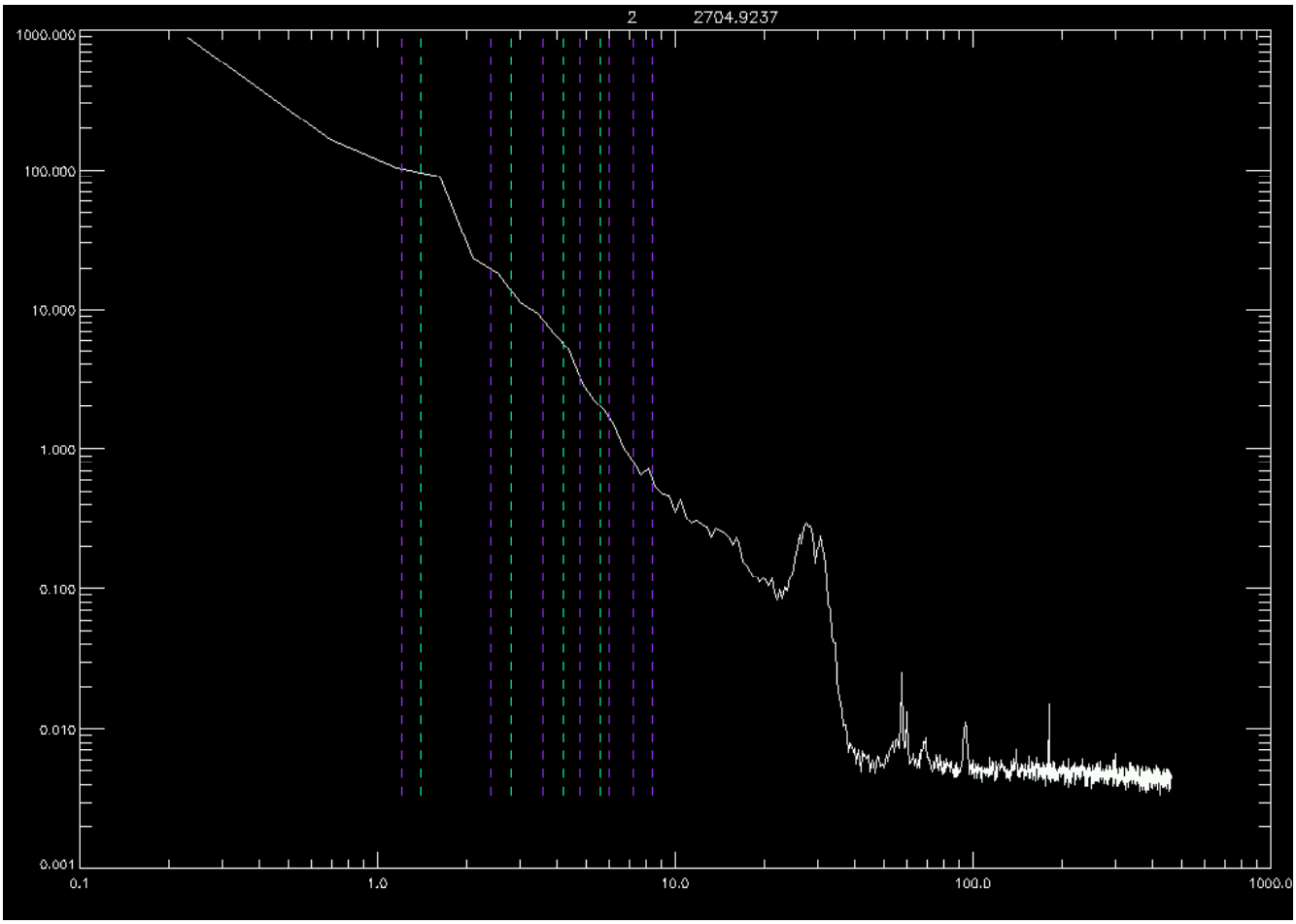

Power spectrum of TPAR_02 s.49, 3rd PC

Finally, the following figure shows the distribution of eigenvalues for this scan, which gives an idea of what the important components of the overall noise are. The first principal component (common mode) stands out well above the rest; the next 8-9 are quite significant, and are all individual-pixel-dominated eigenvectors with strong 1/f power spectra.

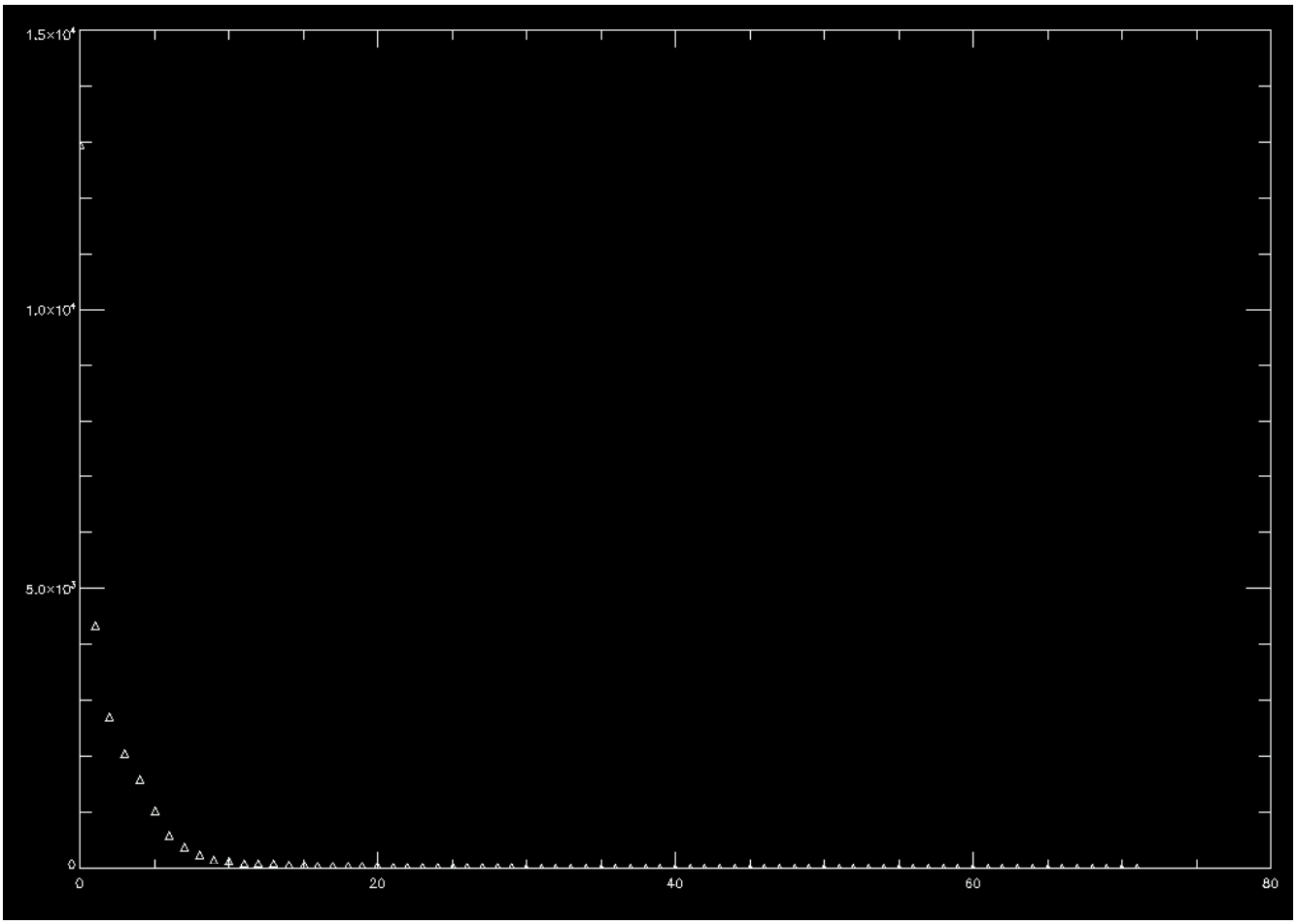

Distribution of eigenvalues of the covariance matrix